# Hidden scale invariance in the Gay-Berne model. II.
# Smectic B phase

Saeed Mehri, Jeppe C. Dyre,* and Trond S. Ingebrigtsen†

*Glass and Time, IMFUFA, Department of Science and Environment,*
*Roskilde University, P.O. Box 260, DK-4000 Roskilde, Denmark*
(Dated: March 7, 2023)

This paper complements a previous study of the isotropic and nematic phases of the Gay-Berne liquid-crystal model [Mehri *et al.*, Phys. Rev. E **105**, 064703 (2022)] with a study of its smectic B phase found at high density and low temperatures. We find also in this phase strong correlations between the virial and potential-energy thermal fluctuations, reflecting hidden scale invariance which implies the existence of isomorphs. The predicted approximate isomorph invariance of the physics is confirmed by simulations of the standard and orientational radial distribution functions, the mean-square displacement as a function of time, as well as the force, torque, velocity, angular velocity, and orientational time-autocorrelation functions. The regions of the Gay-Berne model that are relevant for liquid-crystal experiments can thus fully be simplified via the isomorph theory.

## I. INTRODUCTION

Liquid crystals involve molecules with a high degree of shape anisotropy [1, 2]. This interesting state of matter is relevant in many different contexts, ranging from display applications to biological systems [3–5]. Depending on temperature and pressure, the molecular anisotropy leads to different structural phases, e.g., nematic and smectic phases with long-range orientational ordering [1].

Gay-Berne (GB) models describe molecules of varying shape anisotropy spanning from elongated ellipsoids to thin disks, and GB models have become standard liquid-crystal models [6]. The GB pair potential depends on four dimensionless parameters, which is reflected in the notation $\mathrm{GB}(\kappa, \kappa', \mu, \nu)$ where the four parameters quantify the shape of the molecules and the strength of their interactions. A previous paper studied the isotropic and nematic phases of a GB model with parameters corresponding to rod-shaped elongated molecules [7]. It was found that this model has isomorphs in the isotropic and nematic phases, which are curves in the thermodynamic phase diagram along which the physics is approximately invariant. This paper presents a study of the same GB model that focuses on the smectic B region, demonstrating that isomorphs also exist in this phase.

## II. THE GAY-BERNE POTENTIAL AND SIMULATION DETAILS

The $\mathrm{GB}(\kappa, \kappa', \mu, \nu)$ pair potential is characterized by the following four dimensionless parameters: $\kappa \equiv \sigma_e/\sigma_s$ where $\sigma_e$ and $\sigma_s$ are lengths, $\kappa' \equiv \varepsilon_{ss}/\varepsilon_{ee}$ where $\varepsilon_{ss}$ and $\varepsilon_{ee}$ are energies, and two exponents $\mu$ and $\nu$. The GB pair potential $v_{\mathrm{GB}}$ is defined as follows [6]

$$v_{\mathrm{GB}}(\mathbf{r}_{ij}, \hat{\mathbf{e}}_i, \hat{\mathbf{e}}_j) = 4\varepsilon(\hat{\mathbf{r}}, \hat{\mathbf{e}}_i, \hat{\mathbf{e}}_j) \left[ (\sigma_s/\rho_{ij})^{12} - (\sigma_s/\rho_{ij})^6 \right], \tag{1a}$$

$$\rho_{ij} = r_{ij} - \sigma(\hat{\mathbf{r}}, \hat{\mathbf{e}}_i, \hat{\mathbf{e}}_j) + \sigma_s. \tag{1b}$$

Here, $r_{ij}$ is the distance between molecules $i$ and $j$, $\hat{\mathbf{r}} \equiv \mathbf{r}_{ij}/r_{ij}$ is the unit vector from molecule $i$ to molecule $j$, and $\hat{\mathbf{e}}_i$ and $\hat{\mathbf{e}}_j$ are unit vectors along the major axes of molecules $i$ and $j$. The GB molecule mimics an ellipsoid of two diameters $\sigma_s$ and $\sigma_e$. One defines

$$\sigma(\hat{\mathbf{r}}, \hat{\mathbf{e}}_i, \hat{\mathbf{e}}_j) = \sigma_s \left[ 1 - \frac{\chi}{2} \left( \frac{(\hat{\mathbf{e}}_i \cdot \hat{\mathbf{r}} + \hat{\mathbf{e}}_j \cdot \hat{\mathbf{r}})^2}{1 + \chi(\hat{\mathbf{e}}_i \cdot \hat{\mathbf{e}}_j)} + \frac{(\hat{\mathbf{e}}_i \cdot \hat{\mathbf{r}} - \hat{\mathbf{e}}_j \cdot \hat{\mathbf{r}})^2}{1 - \chi(\hat{\mathbf{e}}_i \cdot \hat{\mathbf{e}}_j)} \right) \right]^{-1/2}, \tag{2a}$$

$$\chi = \frac{\kappa^2 - 1}{\kappa^2 + 1}. \tag{2b}$$

---

* dyre@ruc.dk
† trondingebrigtsen@hotmail.com

Here $\chi$ is a shape anisotropy parameter and $\kappa$ quantifies the molecular asymmetry such that $\kappa = 1$ ($\chi = 0$) represents spherical molecules, $\kappa \to \infty$ ($\chi \to 1$) corresponds to very long rods, and $\kappa \to 0$ ($\chi \to -1$) corresponds to very thin disks. The energy term is given by

$$\varepsilon(\hat{\mathbf{r}}, \hat{\mathbf{e}}_i, \hat{\mathbf{e}}_j) = \varepsilon_0 \left(\varepsilon_1(\hat{\mathbf{e}}_i, \hat{\mathbf{e}}_j)\right)^\nu \left(\varepsilon_2(\hat{\mathbf{r}}, \hat{\mathbf{e}}_i, \hat{\mathbf{e}}_j)\right)^\mu \tag{3a}$$

in which

$$\varepsilon_1(\hat{\mathbf{e}}_i, \hat{\mathbf{e}}_j) = \left(1 - \chi^2(\hat{\mathbf{e}}_i \cdot \hat{\mathbf{e}}_j)^2\right)^{-1/2}, \tag{3b}$$

$$\varepsilon_2(\hat{\mathbf{r}}, \hat{\mathbf{e}}_i, \hat{\mathbf{e}}_j) = 1 - \frac{\chi'}{2}\left(\frac{(\hat{\mathbf{e}}_i \cdot \hat{\mathbf{r}} + \hat{\mathbf{e}}_j \cdot \hat{\mathbf{r}})^2}{1 + \chi'(\hat{\mathbf{e}}_i \cdot \hat{\mathbf{e}}_j)} + \frac{(\hat{\mathbf{e}}_i \cdot \hat{\mathbf{r}} - \hat{\mathbf{e}}_j \cdot \hat{\mathbf{r}})^2}{1 - \chi'(\hat{\mathbf{e}}_i \cdot \hat{\mathbf{e}}_j)}\right). \tag{3c}$$

Here

$$\chi' = \frac{\kappa'^{1/\mu} - 1}{\kappa'^{1/\mu} + 1} \tag{3d}$$

is an energy anisotropy parameter. The energies $\varepsilon_{ss}$ and $\varepsilon_{ee}$ are the well depths of the potential in the side-side and end-end configurations, respectively. Unless otherwise stated, $\sigma_s$ defines the length and $\varepsilon_0$ the energy units used.

We simulated a system of 1372 particles of the GB$(3, 5, 2, 1)$ model studied previously in Ref. 7. The GB pair potential was cut and shifted at $r_c = 4.0$ and the time step used was $\Delta t = 0.001$. The standard $NVT$ Nose-Hoover algorithm was used for the center-of-mass motion and the Fincham algorithm was used for the rotational motion [8]. Different thermostats were applied for the translational and the rotational motions [7]. The molecular moment of inertia was set to unity. A home-made code for GPU computing was used; at each simulated state point 20 million time steps were taken to equilibrate the system before the production run of 67 million time steps.

The GB(3,5,2,1) phase diagram is shown in Fig. 3 of Ref. 7. Figure 1 shows a snapshot of the system at equilibrium in the smectic B phase.
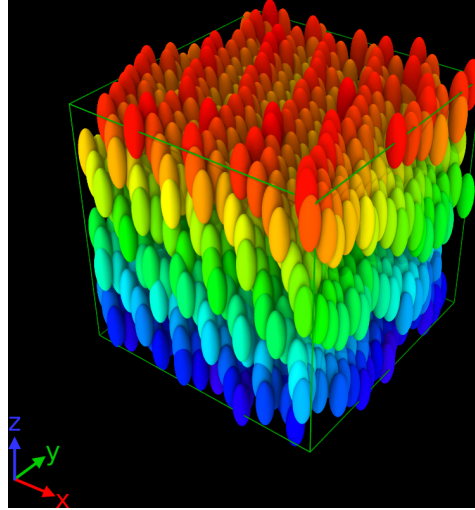


FIG. 1. Snapshot of the smectic B phase at density 0.4 and temperature 1.2. A color coding is introduced here to visualize the individual planes.

### III. PROPERTIES STUDIED

The quantities evaluated in this study were the following: the standard radial distribution function $g(r)$ [9, 10], the below defined orientational radial distribution function $G_l(r)$ ($l = 2$) [10–12], as well as several single-molecule time-autocorrelation functions [13, 14]. The latter two observables are defined by

$$G_l(r) \equiv \langle P_l(\hat{\mathbf{e}}_i \cdot \hat{\mathbf{e}}_j)\rangle, \tag{4}$$

$$\phi_A(t) = \langle \mathbf{A}(t_0) \cdot \mathbf{A}(t_0 + t)\rangle. \tag{5}$$

Here $P_l$ is the Legendre polynomial, $\mathbf{A}(t)$ is a vector defined for each molecule, and the angular brackets denote an ensemble and particle average that in the case of $G_l(r)$ is restricted to including pairs of particles of distance $r$. We study $\mathbf{A}$ equal to the individual particles' velocity, angular velocity, force, and torque. We also study the first- and second-order molecular orientational order parameter time-autocorrelation functions defined by

$$\phi_l(t) = \langle P_l(\hat{\mathbf{e}}_i(t_0) \cdot \hat{\mathbf{e}}_i(t_0 + t)) \rangle. \tag{6}$$

## IV. R-SIMPLE SYSTEMS AND ISOMORPHS

The virial $W$ quantifies the part of the pressure $p$ that derives from molecular interactions via the defining identity $pV = Nk_BT + W$, in which $V$ is the volume and $N$ is the number of molecules [15]. Liquids and solids may be classified according to the degree of correlation between the constant-volume thermal-equilibrium fluctuations of virial $W$ and potential energy $U$ [16]. "R-simple systems" are defined as those with strong $WU$ correlations; such systems are particularly simple because their thermodynamic phase diagram is basically one-dimensional in regard to structure and dynamics [16–19]. The "isomorph theory" of R-simple systems was developed over the last decade [20–23].

The $WU$ Pearson correlation coefficient, which depends on the state point in question, is defined by

$$R = \frac{\langle \Delta W \Delta U \rangle}{\sqrt{\langle (\Delta W)^2 \rangle \langle (\Delta U)^2 \rangle}}. \tag{7}$$

Here $\Delta$ gives the deviation from the equilibrium mean value and $\rho \equiv N/V$ is the particle density. Many systems, including the standard Lennard-Jones and Yukawa fluids, have strong $WU$ correlations in their liquid and solid phases, whereas $R$ usually decreases significantly for densities below the critical density [24]. A system is considered to be R-simple whenever $R > 0.9$ at the state points of interest [25]. This is a pragmatic criterion, however, and, e.g., the simulations presented in this paper go below this value at high temperatures without significantly affecting the degree of isomorph invariance.

As mentioned, R-simple systems have curves in the phase diagram along which structure and dynamics are approximately invariant. These curves are termed *isomorphs*. Isomorph invariance applies when data are presented in so-called reduced units. These units, which in contrast to ordinary units are state-point dependent, are given by letting the density $\rho$ define the length unit $l_0$, the temperature define the energy unit $e_0$, and density and thermal velocity define the time unit $t_0$,

$$l_0 = \rho^{-1/3}, \quad e_0 = k_BT, \quad t_0 = \rho^{-1/3}\sqrt{m/k_BT}. \tag{8}$$

Here $m$ is the molecule mass. Quantities given in isomorph-theory reduced units are marked with a tilde.

Strong virial potential-energy correlations arise whenever hidden scale invariance applies. This is the condition that the potential-energy ordering of same-density configurations is maintained under a uniform scaling of all coordinates [26], which is formally expressed as follows

$$U(\mathbf{R}_a) < U(\mathbf{R}_b) \Rightarrow U(\lambda\mathbf{R}_a) < U(\lambda\mathbf{R}_b). \tag{9}$$

Here $\mathbf{R} \equiv (\mathbf{r}_1, ..., \mathbf{r}_N)$ is the vector of all particle coordinates and $\lambda$ is a scaling factor. Consider two configurations with the same potential energy, i.e., $U(\mathbf{R}_a) = U(\mathbf{R}_b)$. After a uniform scaling one has by Eq. (9) $U(\lambda\mathbf{R}_a) = U(\lambda\mathbf{R}_b)$. By taking the derivative of this with respect to $\lambda$ one derives $W(\mathbf{R}_a) = W(\mathbf{R}_b)$ [26]. Thus same potential energy implies same virial, implying a 100% correlation between $W$ and $U$ constant-volume fluctuations. For realistic systems Eq. (9) applies only approximately, however, and in practice one rarely experiences perfect virial potential-energy correlations (which only applies when $U(\mathbf{R})$ is an Euler-homogeneous function).

Recall that a system's entropy $S$ is that of an ideal gas at the same density and temperature, $S_{id}$, plus an "excess" term, $S_{ex}$, deriving from the intermolecular interactions: $S = S_{id} + S_{ex}$. It can be shown that Eq. (9) implies that the reduced-unit structure and dynamics are invariant along the lines of constant excess entropy; these are by definition the system's isomorphs [26]. The so-called density-scaling exponent $\gamma$ is defined by

$$\gamma \equiv \left( \frac{\partial \ln T}{\partial \ln \rho} \right)_{S_{ex}} = \frac{\langle \Delta W \Delta U \rangle}{\langle (\Delta U)^2 \rangle}. \tag{10}$$

| $\rho$ | $T$ | $R$ | $\gamma$ |
|-------|-------|-------|-------|
| 0.400 | 0.400 | 0.956 | 9.46 |
| 0.416 | 0.578 | 0.946 | 9.04 |
| 0.433 | 0.823 | 0.936 | 8.74 |
| 0.451 | 1.160 | 0.925 | 8.50 |
| 0.469 | 1.619 | 0.905 | 8.28 |
| 0.488 | 2.240 | 0.887 | 8.06 |
| 0.508 | 3.079 | 0.868 | 7.92 |
| 0.529 | 4.211 | 0.854 | 7.85 |
| 0.550 | 5.770 | 0.854 | 8.00 |

TABLE I. Variation of density $\rho$, temperature $T$, virial potential-energy correlation coefficient $R$ (Eq. (7)), and density-scaling exponent $\gamma$ (Eq. (10)) for nine state points on the isomorph generated from the reference state point $(\rho, T) = (0.4, 0.4)$.

The second equality is a general identity [21], which is particularly useful when the system is R-simple because Eq. (10) can then be used for tracing out isomorphs without knowing the equation of state. For the simple Euler algorithm this is done by proceeding as follows. At a given state point $(\rho_1, T_1)$, by means of Eq. (10) one calculates $\gamma$ from the equilibrium fluctuations of potential energy and virial. From Eq. (10) one then predicts the temperature $T_2$ with the property that $(\rho_2, T_2)$ is on the same isomorph as $(\rho_1, T_1)$. If $\gamma = 4$, for instance, for a one percent density increase a four percent temperature increase will ensure that the new state point is on the same isomorph. In the simulations of this paper, however, in order to increase the accuracy of the generated isomorph, following Ref. 27 we used instead the fourth-order Runge-Kutta algorithm for solving numerically Eq. (10) (involving density changes of order 1% ). The resulting isomorph state points for which data are given below are reported in Table I.
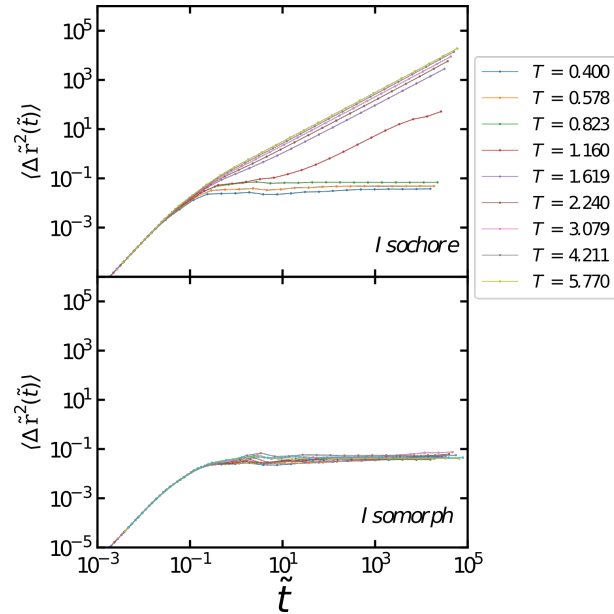


FIG. 2. Reduced-unit mean-square displacement as function of time along the $\rho = 0.4$ isochore and along the isomorph generated from the reference state point $(\rho, T) = (0.4, 0.4)$ (Table I). The colors used here for the different temperatures are also used in Figs. 3-6.

## V. STRUCTURE AND DYNAMICS MONITORED ALONG AN ISOCHORE AND AN ISOMORPH

We begin the study by presenting results for the mean-square displacement as a function of time, which is predicted to be isomorph invariant in reduced units. Figure 2 shows the results along the $\rho = 0.4$ isochore (upper panel) and along the isomorph generated from the reference state point $(\rho, T) = (0.4, 0.4)$ (lower panel), in both cases for the same nine temperatures. The isomorph data involve state points of more than a factor of a third density change and more than a factor of ten temperature change (Table I).

The low-temperature state points along the isochore of Fig. 2 are in the solid state as evident from the fact that the long-time mean-square displacement is constant. The high-temperature isochore state points, on the other hand, are liquid by showing diffusive long-time behavior. The fact that all mean-square displacement data collapse at short times in the ballistic regime for both the isochore and the isomorph is a straightforward consequence of the use of reduced units because this leads to a reduced-unit thermal velocity that is the same at all state points. For the isomorph data, we see a fairly good collapse at all times, not just at short times. The deviations from perfect collapse derive from the fact that the virial potential-energy correlation coefficient $R$ is not close to unity; in fact, $R$ goes below 0.9 at the four highest temperatures (Table I).

Figure 3 shows reduced-unit data for the radial distribution function $g(r)$ and the orientational radial distribution function $G_2(r)$ (Eq. (4)) along the same isochore and isomorph. Figure 3 shows no invariance along the isochore, but a fair invariance along the isomorph. An exception to this is the highest temperature isomorph radial distribution function that deviates notably from the eight others. We have found that at this (and higher) temperatures, the smectic B phase undergoes a further transition involving a tilt of the average molecular orientation with respect to the smectic layers, similar to what has been reported by de Miguel *et al.* [10]. Interestingly, this does not seem to affect the isomorph invariance of other quantities than the radial distribution function, compare the $G_2(r)$ data of Fig. 3 and the data of later figures.
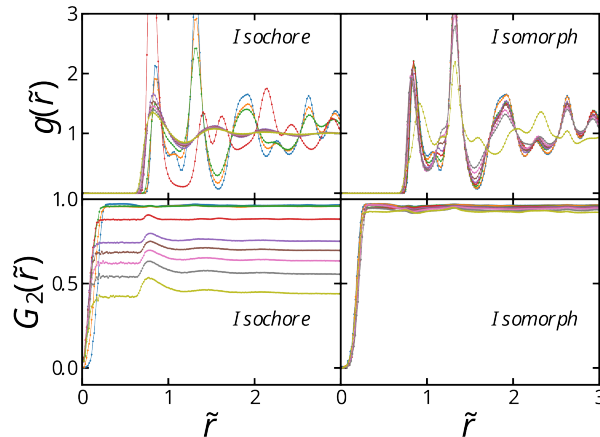


FIG. 3. Structure along the isochore and the isomorph probed via the standard radial distribution function (upper panels) and the orientational radial distribution function defined in Eq. (4) (lower panels), in both cases plotted as a function of the reduced pair distance $\tilde{r}$.

Returning to dynamic properties, the normalized force and torque time-autocorrelation functions are shown in Fig. 4 as functions of the reduced time. Near-perfect scaling is observed for both functions along the isomorph.
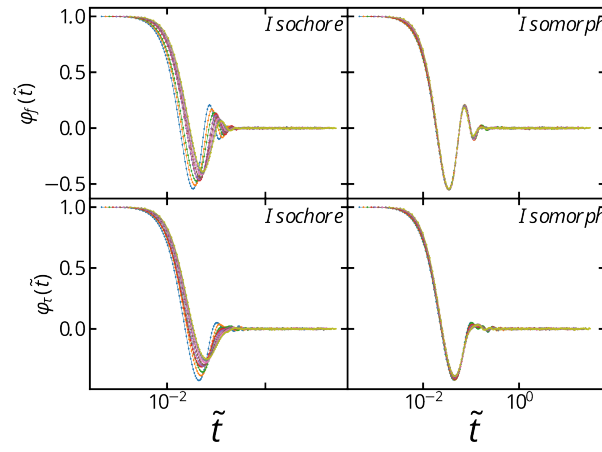
FIG. 4. Normalized force (upper panels) and torque (lower panels) time-autocorrelation functions along the same isochore and isomorph as in the previous figures, plotted as functions of the reduced time $\tilde{t}$.

Figure 5 shows the first- and second-order orientational time-autocorrelation functions along the isochore and the isomorph. These functions both decay to zero at the highest density studied on the isochore, which is not the case for the isomorph along which invariant dynamics is observed.
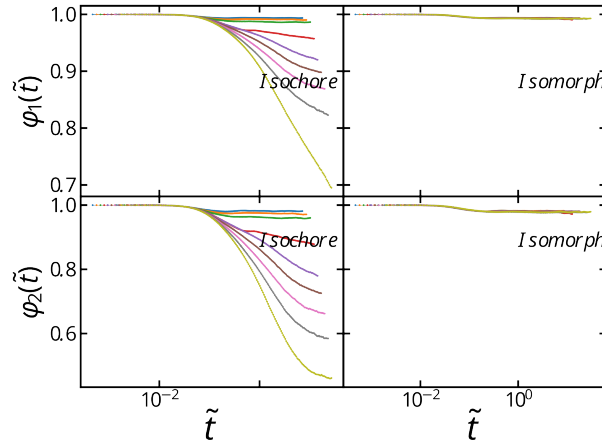


FIG. 5. First- and second-order orientational order parameter time-autocorrelation functions along the isochore and isomorph, plotted as functions of the reduced time.

We finish the study by showing the normalized velocity and angular velocity time-autocorrelation functions in Fig. 6. Again, good isomorph invariance is observed at all times, though with some deviation at intermediate times fo the velocity time-autocorrelation function.
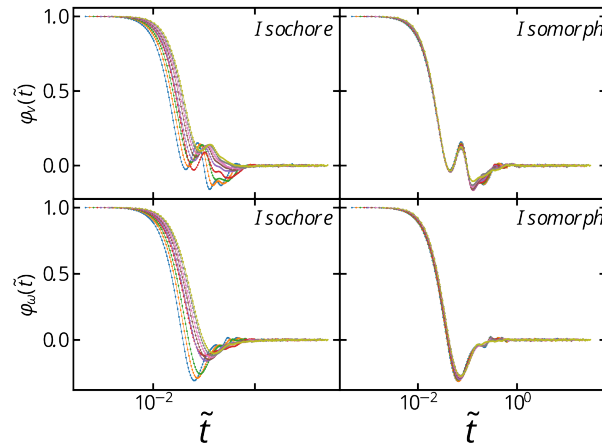
FIG. 6. Normalized velocity and angular velocity time-autocorrelation functions along the isochore and isomorph, plotted as functions of the reduced time.

## VI. SUMMARY

We have shown that the isomorph theory can be used to understand GB liquid crystals in the smectic B phase, because the thermodynamic phase diagram is here effectively one-dimensional in the sense that the reduced-unit structure and dynamics are approximately invariant along the isomorphs. The previous paper [7] showed that the same applies for the isotropic and nematic phases of the GB(3,5,2,1) model. This means that the GB(3,5,2,1) phase diagram is effectively one-dimensional in regard to structure and dynamics. We note that this property is not limited to this particular GB model; thus an earlier publication demonstrated the existence of isomorphs in the GB(0.345,0.2,1,2) model that forms a discotic liquid-crystal phase at low temperatures [28].

Specifically, we showed above that the GB(3,5,2,1) model exhibits good invariance of the reduced-unit structure and dynamics along the studied isomorph. In conjunction with our previous study [7], the existence of isomorphs in the GB model can now be used to explain the observed behavior of liquid crystals, for instance the so-called density scaling, which is the fact that the reduced-unit dynamics is invariant along lines of constant $\rho^\gamma/T$ [29, 30]. Studies remain to investigate whether other smectic phases of the GB model also exhibit strong virial potential-energy correlations and thus the existence of isomorphs. Also, it would be interesting to investigate systematically the vast parameter space of the GB potential from a hidden-scale-invariance perspective.

## ACKNOWLEDGMENTS

[1] P. G. de Gennes and J. Prost, *The Physics of Liquid Crystals*, 2nd ed. (Oxford Science Publications, 1993).

[2] M. Jurásek and R. Vácha, Self-assembled clusters of patchy rod-like molecules, Soft Matter **13**, 7492 (2017).

[3] S. J. Woltman, G. P. Crawford, and G. D. Jay, *Liquid crystals: frontiers in biomedical applications* (World Scientific, 2007).

[4] A. de la Cotte, C. Wu, M. Trevisan, A. Repula, and E. Grelet, Rod-like virus-based multiarm colloidal molecules, ACS Nano **11**, 10616 (2017).

[5] Y. Tian and Z. Niu, Self-assembly of rod-like bionanoparticles at interfaces and in solution, in *Virus-Derived Nanoparticles for Advanced Technologies* (Springer, 2018).

[6] J. Gay and B. Berne, Modification of the overlap potential to mimic a linear site–site potential, J. Chem. Phys. **74**, 3316 (1981).

[7] S. Mehri, J. C. Dyre, and T. S. Ingebrigtsen, Hidden scale invariance in the Gay-Berne model, Phys. Rev. E **105**, 064703 (2022).

[8] D. Fincham, More on rotational motion of linear molecules, CCP5 Quarterly **12**, 47 (1984).

[9] M. Bates and G. Luckhurst, Computer simulation studies of anisotropic systems. xxx. the phase behavior and structure of a Gay-Berne mesogen, J. Chem. Phys. **110**, 7087 (1999).

[10] E. De Miguel, L. F. Rull, M. K. Chalam, and K. E. Gubbins, Liquid crystal phase diagram of the Gay-Berne fluid, Mol. Phys. **74**, 405 (1991).

[11] E. de Miguel, L. F. Rull, M. K. Chalam, K. E. Gubbins, and F. Van Swol, Location of the isotropic-nematic transition in the Gay-Berne model, Mol. Phys. **72**, 593 (1991).

[12] D. Adams, G. Luckhurst, and R. Phippen, Computer simulation studies of anisotropic systems: XVII. The Gay-Berne model nematogen, Mol. Phys. **61**, 1575 (1987).

[13] E. de Miguel, L. F. Rull, and K. E. Gubbins, Dynamics of the Gay-Berne fluid, Phys. Rev. A **45**, 3813 (1992).

[14] P. P. Jose and B. Bagchi, Multiple short time power laws in the orientational relaxation of nematic liquid crystals, J. Chem. Phys. **125**, 184901 (2006).

[15] N. P. Bailey, L. Bøhling, A. A. Veldhorst, T. B. Schrøder, and J. C. Dyre, Statistical mechanics of Roskilde liquids: Configurational adiabats, specific heat contours, and density dependence of the scaling exponent, J. Chem. Phys. **139**, 184506 (2013).

[16] T. S. Ingebrigtsen, T. B. Schrøder, and J. C. Dyre, What is a simple liquid?, Phys. Rev. X **2**, 011011 (2012).

[17] T. S. Ingebrigtsen, T. B. Schrøder, and J. C. Dyre, Isomorphs in model molecular liquids, J. Phys. Chem. B **116**, 1018 (2012).

[18] J. C. Dyre, Hidden scale invariance in condensed matter, J. Phys. Chem. B **118**, 10007 (2014).

[19] J. C. Dyre, Perspective: Excess-entropy scaling, J. Chem. Phys. **149**, 210901 (2018).

[20] N. P. Bailey, U. R. Pedersen, N. Gnan, T. B. Schrøder, and J. C. Dyre, Pressure-energy correlations in liquids. I. results from computer simulations, J. Chem. Phys. **129**, 184507 (2008).

[21] N. Gnan, T. B. Schrøder, U. R. Pedersen, N. P. Bailey, and J. C. Dyre, Pressure-energy correlations in liquids. IV. "Isomorphs" in liquid phase diagrams, J. Chem. Phys. **131**, 234504 (2009).

[22] A. A. Veldhorst, J. C. Dyre, and T. B. Schrøder, Scaling of the dynamics of flexible Lennard-Jones chains, J. Chem. Phys. **141**, 054904 (2014).

[23] L. Costigliola, T. B. Schrøder, and J. C. Dyre, Freezing and melting line invariants of the Lennard-Jones system, Phys. Chem. Chem. Phys. **18**, 14678 (2016).

[24] I. H. Bell, R. Messerly, M. Thol, L. Costigliola, and J. C. Dyre, Modified entropy scaling of the transport properties of the Lennard-Jones fluid, J. Phys. Chem. B **123**, 6345 (2019).

[25] N. P. Bailey, U. R. Pedersen, N. Gnan, T. B. Schrøder, and J. C. Dyre, Pressure-energy correlations in liquids. I. Results from computer simulations, J. Chem. Phys. **129**, 184507 (2008).

[26] T. B. Schrøder and J. C. Dyre, Simplicity of condensed matter at its core: Generic definition of a Roskilde-simple system, J. Chem. Phys. **141**, 204502 (2014).

[27] E. Attia, J. C. Dyre, and U. R. Pedersen, Extreme case of density scaling: The Weeks-Chandler-Andersen system at low temperatures, Phys. Rev. E **103**, 062140 (2021).

[28] S. Mehri, M. A. Kolmangadi, J. C. Dyre, and T. S. Ingebrigtsen, Lines of invariant physics in the isotropic phase of the discotic Gay-Berne model, J. Non-Cryst. Solids: X **14**, 100085 (2022).

[29] C. M. Roland, S. Hensel-Bielowka, M. Paluch, and R. Casalini, Supercooled dynamics of glass-forming liquids and polymers under hydrostatic pressure, Rep. Prog. Phys. **68**, 1405 (2005).

[30] K. Satoh, Characteristic behavior of short-term dynamics in reorientation for Gay-Berne particles near the nematic-isotropic phase transition temperature, J. Chem. Phys. **125**, 204902 (2006).